J Fluoresc (2014) 24:1629–1638
DOI 10.1007/s10895-014-1449-1

ORIGINAL PAPER

Spectroscopic Investigation, Effect of Solvent Polarity and Fluorescence Quenching of a New D-π-A Type Chalcone Derivative

Mehboobali Pannipara · Abdullah M. Asiri · Khalid A. Alamry · Muhammad N Arshad · Samy A. El-Daly

Received: 14 July 2014 / Accepted: 20 August 2014 / Published online: 30 August 2014

Abstract A new chalcone derivative 3-(1-methyl-1H-pyrrol-2-yl)-1-naphthalen-2-yl propenone (MPNP) with electron donor-acceptor group has been synthesized and characterized by IR, ^{1}HNMR, ^{13}C NMR and X- ray crystallography. Electronic absorption and emission spectra of MPNP have been studied in solvents of different polarity. A remarkable red shift was observed in the emission spectrum of MPNP compared to the absorption spectrum upon increasing the solvent polarity, indicating a higher dipole moment in the excited state than in the ground state and the transition involved are π-π* with charge transfer character. Lippert-Mataga and Reichardts correlations were used to estimate the change in dipole moments ($\Delta\mu$); suggest that the emissive state of MPNP is of strong ICT character. Fluorescence quantum yield (ϕ_f) of MPNP was correlated with empirical solvent polarity parameter $E_T(30)$, and it is observed that ϕ_f increases with increase in solvent polarity of polar aprotic solvents and decrease in alcoholic solvents. The interaction of MPNP with colloidal silver nanoparticles (AgNPs) was also studied in ethanol and ethylene glycol using steady state emission measurements. The fluorescence quenching data reveal that dynamic quenching and energy transfer play a major role in the fluorescence quenching of MPNP by Ag NPs.

Keywords Chalcone · Effect of solvents · Physicochemical parameters · Fluorescence quenching · Ag nanoparticles

Introduction

The photophysical properties of pi-conjugated organic fluorophores containing donor acceptor groups that are separated by an ethenyl or keto-vinyl bridge are of continuing theoretical and experimental research because of their rapidly expanding applications in a variety of areas, such as dye lasers, sensors, and nonlinear optical materials [1–3]. The electron acceptor group in a pi-conjugated organic molecule withdraws electronic charge from the electron donor group through the conjugated bridge, resulting in polarization of the pi electron skeleton. The photophysical properties of this class of organic compounds originate mainly from the donor-acceptor interaction and high level of the pi-conjugated charge transfer. Hence, conjugated organic compounds are good candidates to a great extent, as it can be tuned and tailored by structural modification for their potential applications in organic optoelectronic devices such as organic field-effect transistors (OFET), organic light emitting diodes (OLEDs), and other all optical devices [4–6].

Chalcones are a class of compounds in which two aromatic planar rings are connected through a α, β-unsaturated carbonyl system with strong electron donor-acceptor interactions depending on the substituent attached to the aromatic rings. Apart from very important biological and pharmaceutical applications, the photophysical properties of chalcones have attracted considerable research attention including metal sensing, optical materials, laser dyes, etc. [7–9]. The photophysical

Electronic supplementary material The online version of this article (doi:10.1007/s10895-014-1449-1) contains supplementary material, which is available to authorized users.

M. Pannipara · A. M. Asiri · K. A. Alamry · M. N. Arshad · S. A. El-Daly (✉)
Department of Chemistry, Faculty of Science, King Abdulaziz University, P.O. Box 80203, Jeddah 21589, Saudi Arabia
e-mail: samyeldaly@yahoo.com

A. M. Asiri · M. N. Arshad
Center of Excellence for Advanced Materials Research, King Abdulaziz University, Jeddah 21589P.O. Box 80203, Saudi Arabia

S. A. El-Daly
Department of Chemistry, Faculty of Science, Tanta University, 31527 Tanta, Egypt

properties of these pi-conjugated compounds originate mainly from the intramolecular charge transfer state that depends strongly on the substituent effect and properties of solvents.

Interaction of metallic nanoparticles (NPs) with fluorophores has become an active area of research for the last two decades with applications ranging from material science to biomedical science [10–12]. The fluorescence of a dye molecule is quenched or enhanced in the close proximity of the metallic nanoparticles and these phenomena can be used for sensing or molecular imaging applications [13, 14]. The emission behavior of a dye molecule can be altered by using metallic nanoparticles having a plasmonic resonance in the visible wavelength region such as gold and silver. Quenching or enhancement of photoluminescence of a dye by silver nanoparticles (AgNPs) depends upon the distance between the dye molecule and NPs [15–17]. The quenching processes are of three types: static, dynamic and by electron/energy transfer. In static quenching, the decrease in emission intensity is caused by the adsorption of dye molecule on the surface of metallic NPs, forming a non fluorescent complex between the fluorophore and quencher where as in dynamic quenching; the reduction of emission intensity is due to the direct interaction or collision of excited fluorophore with a quencher during their excited state life time. The third type of quenching process takes place by non-radiative energy / electron transfer between the dye molecule and NPs [18, 19]. The quenching of fluorescence dominates over enhancement at shorter distances and it is attributed to the efficient non radiative energy transfer between the dye molecule and the metallic NP [20].

Recently, our research group have been devoted to synthesis of novel chalcone derivatives and diolefinic compounds containing donor-acceptor group for to investigate their spectral and photophysical properties [1, 21]. In the present communication, we report on the spectral behavior of 3-(1-methyl-1H-pyrrol-2-yl)-1-naphthalen-2-yl propenone (MPNP) in different solvents and its fluorescence quenching by silver nanoparticles. The aim of this study is to perform a detailed investigation on the spectral characterization and photophysical properties of this donor-acceptor type chalcone derivative in different media.

Experimental

Materials

Synthetic procedure and characterization of MPNP by IR, ^{1}HNMR, ^{13}C NMR are given in the supporting information and synthetic route is outlined in Scheme. 1. 1-methylpyrrole-2-carboxaldehyde and 2-acetonaphthone were purchased from Sigma-Aldrich. All solvents and chemicals used in this work were of spectroscopic grade obtained from Sigma Aldrich and used without further purification.

X-Ray Single Crystal

Single crystal of MPNP suitable for X-ray analysis was obtained at room temperature by slow evaporation of chloroform solution. One crystal of MPNP (orange 0.33×0.25×0.09 mm) was mounted on Agilent Supernova (Dual source) Agilent Technologies Diffract meter, equipped with a graphite-monochromatic CuKα radiation (λ=1.54184), to collect diffraction data using CrysAlisPro software at 296 K. The structure solution was achieved through computer assisted program packages such as, SHELXS–97 [22] and refined by full–matrix least–squares methods on F^2 using SHELXL–97, inbuilt with X-Seed [23]. All the C-H hydrogen atoms were positioned geometrically and treated as riding atoms with $C_{aromatic}$–H=0.93 Å, C_{methyl}–H=0.96 Å and refined using a riding model with Uiso (H)=1.5 Ueq (C) for methyl and Uiso (H)=1.2 Ueq (C) for all other carbon atoms. CCDC (Cambridge Crystallographic Data Centre) reference number 981028 contains the supplementary crystallographic data for this paper. These data can be obtained free of charge at www.ccdc.cam.ac.uk/conts/retrieving.html or from the Cambridge Crystallographic Data Centre, 12 Union Road, Cambridge CB2 1EZ, UK.

Synthesis and Characterization of Silver Nanoparticles

Silver nanoparticles were prepared by the well known chemical reduction method [24]. In a typical procedure, 125 ml of 1 × 10^{-3} M silver nitrate solution was heated to boiling and 5 ml of 1 % trisodium citrate solution (as nucleating and reducing agent) was added quickly. This resulted in a color change from pale yellow to golden yellow indicating the formation of Ag NPs; stirring was continued until cooled to room temperature. The nanoparticles were characterized by using UV–vis absorption spectrophotometer and Transmission Electron Microscope (TEM). A typical solution of 40–45 nm diameter silver nanoparticles having polygonal shape, exhibiting a characteristic surface Plasmon band around 430 nm was obtained. TEM image of Ag NPs with absorption spectrum shown as an inset is shown in Fig. 1.

Spectral Measurements

Solvents were checked for the absence of absorbing or fluorescent impurities within the scanned spectral ranges. UV–vis electronic absorption spectra was recorded on a Shimadzu UV-160A spectrophotometer, and the steady-state fluorescence spectra were measured using Shimadzu RF 5,300 spectrofluorphotometer using a rectangular quartz cell of dimensions 0.2 cm × 1 cm. The emission was monitored at right

Scheme 1 Synthetic route of MPNP

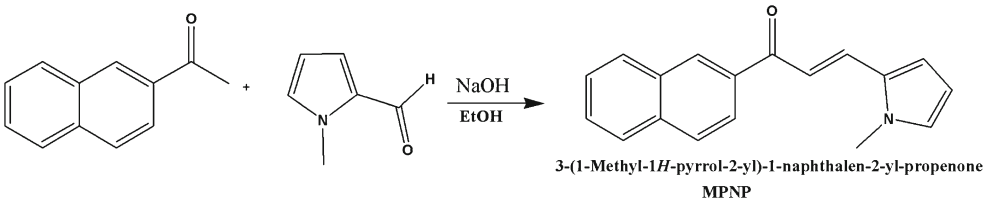

angle. For processing of all sorts of interpretations based upon fluorescence intensity data the necessary corrections for inner filter effect has been done according to the following Eq. (1) [25]:

$$I = I_{obs} \times \exp\left[\frac{1}{2}(A_{ex} + A_{em})\right] \quad (1)$$

Here I is the corrected fluorescence intensity and I_{obs} is the observed background-subtracted fluorescence intensity of the sample under investigation. A_{ex} and A_{em} are the measured absorbance at the excitation and emission wavelengths, respectively. The fluorescence quantum yield (ϕf) was measured using an optically diluted solution of quinine sulfate as reference according to Eq. (2) [25]:

$$\phi_u = \phi_s \times \frac{I_u}{I_s} \times \frac{A_s}{A_u} \times \frac{n_u^2}{n_s^2} \quad (2)$$

where ϕ_u, ϕ_s are the fluorescence quantum yields of the unknown and standard, respectively, I is the integrated emission intensity; A is the absorbance at excitation wavelength, and n is the refractive index of the solvent.

Results and Discussion

Spectral Behavior of MPNP in Different Solvents

The absorption and fluorescence spectra of 1 x 10^{-5} mol L^{-1} MPNP recorded in solvents of different polarity. The absorption and emission spectra of MPNP in few representative solvents are shown in Figs. 2 and 3, respectively and the corresponding spectral data in detail are summarized in Table 1. As seen in Figs. 2 and 3, the compound show a broad absorption band at 385–402 nm on going from heptane to DMSO, while its emission spectrum show two bands, one originating from the locally excited state and the other from the intramolecular charge transfer state (ICT), on excitation at 365 nm. A considerable red shift is observed in the emission spectrum from 435 to 489 nm on changing the solvent polarity from non polar to polar, where as no such shift is observed in the absorption spectrum with varying solvent polarity. Hence, a large difference in the magnitude of Stokes shift is observed that vary from 2,875 to 4,808 cm^{-1}, indicating that excited state geometry of MPNP could be different from that of ground state. It is concluded that emission spectra is more

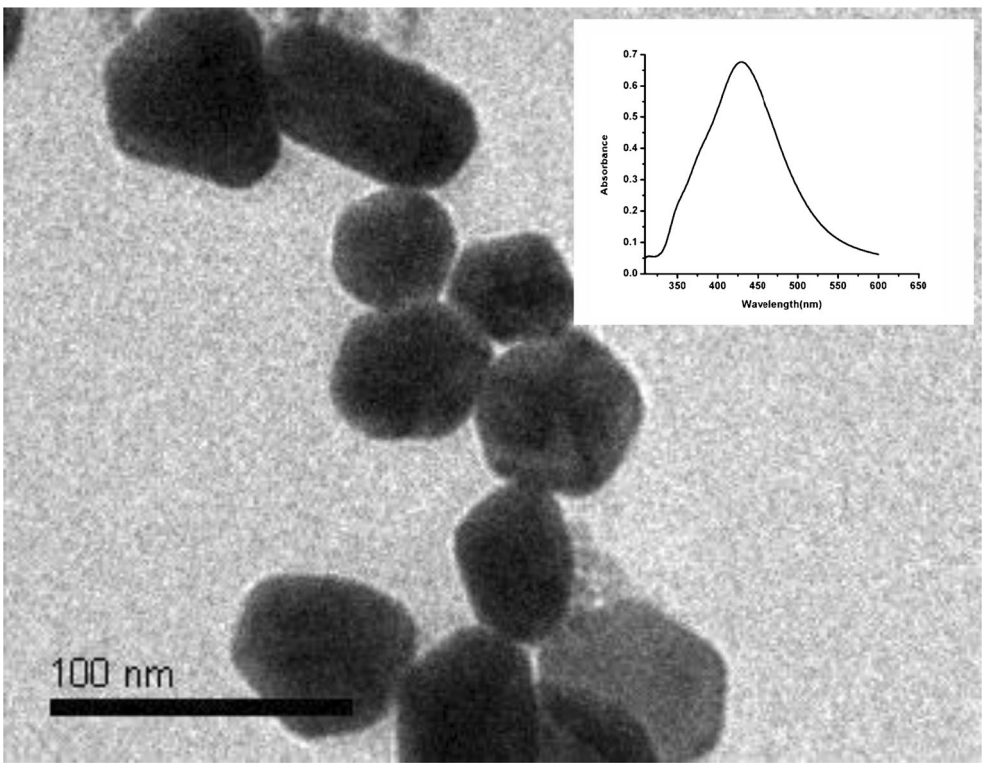

Fig. 1 TEM image of silver nanoparticle. The inset shows the absorption spectrum of Ag NPs

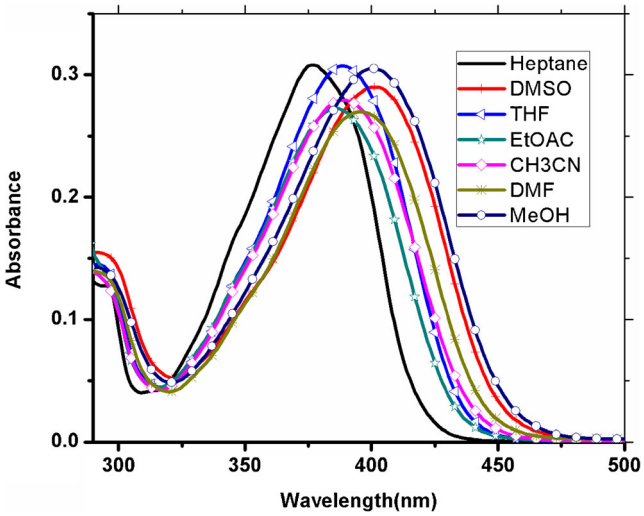

Fig. 2 Electronic absorption spectra of 1×10^{-5} mol L^{-1} of MPNP in different solvents

sensitive to solvent polarity compared to absorption spectra, which indicates that photoinduced intramolecular charge transfer (ICT) occurs in the singlet excited state from the electron donating substituent group to the electron acceptor carbonyl group of chromophore and therefore the polarity of MPNP increases on excitation with a large dipole moment in the excited state than ground state. Moreover, stabilization of highly dipolar excited state in polar solvents confirm the presence of π-π* transitions in MPNP [2, 25–27]. The intensity of the emission spectra of MPNP was found to be highest in polar aprotic solvents that are having high dielectric constant like DMSO and DMF, and lowest in polar protic solvents due to solute-solvent interaction such as hydrogen bonding.

The change in dipole moment between the excited singlet state and the ground state ($\Delta\mu=\mu_e-\mu_g$) of MPNP have been

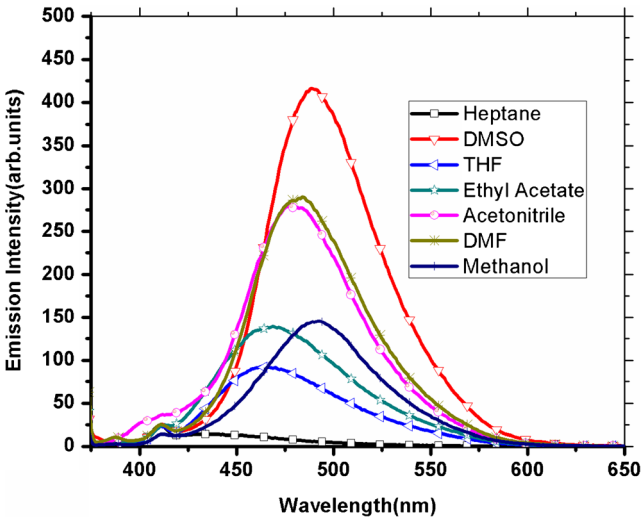

Fig. 3 Emission spectra of 1×10^{-5} mol L^{-1} of MPNP in different solvents

calculated using simplified Lippert-Mataga' Eqs. (3, 4) [28, 29]:

$$\Delta\bar{\nu}_{st} = \frac{2\left(\mu_e - \mu_g\right)^2}{hca^3}\Delta f + Const. \quad (3)$$

$$\Delta f = \frac{\varepsilon - 1}{2\varepsilon + 1} - \frac{n^2-1}{2n^2+1} \quad (4)$$

where $\Delta\bar{\nu}_{st}$ is the difference between the absorption and emission maxima expressed in wave numbers (cm^{-1}), respectively, h is Planck's constant, c is the speed of light in vacuum, a is the Onsager cavity radius, ε and n are the dielectric constant and refractive index of the solvent, respectively, μ_e and μ_g are the dipole moments in the excited and ground state, respectively, and Δf is the orientation polarizability of the solvent which measures both electron mobility and dipole moment of the solvent molecule. The Onsager cavity radii (a) from molecular volume of molecules is calculated by using Suppan's Eq. (5) [30.]

$$a = \left(\frac{3M}{4\pi\delta N}\right)^{1/3} \quad (5)$$

where δ is the density (obtained from crystallographic data) of dye, M is the molecular weight of dye and N is Avogadro's number. The value of (a) for MPNP was found to be 4.34 Å. Figure 4 shows the plot of Stokes shift versus the orientation polarization (Δf), and the change in dipole moment calculated for MPNP from the slop of this plot and cavity radius (a) is found to be 7.09 Debye. The data in polar protic solvents were excluded to avoid specific solute-solvent interactions (hydrogen bonding). This change in dipole moment was caused by redistribution of atomic charges in the excited state due to charge transfer from the electron donor groups to the electron acceptor keto-group.

In addition, the change in dipole moment ($\Delta\mu$) between the excited singlet and ground state was also investigated using solvatochromic shift method [31, 32], making use of the dimensionless microscopic solvent polarity parameters E_T^N given by the Eqs. (6) and (7),

$$E_T^N = \frac{E_T(solvent)-30.7}{32.4} \quad (6)$$

$$E_T(solvent) = \frac{28591}{\lambda_{max}(nm)} \quad (7)$$

where λ_{max} corresponds to the peak wavelength in the red region of the intramolecular charge transfer absorption of the

Table 1 Spectral and photophysical parameters of MPNP in different solvents

Solvents	λ_{abs} (nm)	λ_{em} (nm)	$\Delta\bar{\nu}(cm^{-1})$	ε $M^{-1}cm^{-1}$	Φ_f	f	μ_{12} Debye	E_T (30) K cal mol^{-1}	$\Delta f(D,n)$	E_T^N
Hexane	389	438	2876	28260	0.003	0.57	6.83	31.1	0.0014	0.006
Toluene	389	438	2876	31260	0.020	0.61	7.08	33.9	0.0132	0.099
Heptane	385	435	2986	30810	0.004	0.59	6.91	31.1	0.0004	0.006
DMSO	402	488	4384	28990	0.130	0.57	6.99	45.1	0.263	0.441
Dioxane	389	460	3968	28440	0.023	0.55	6.71	36	0.021	0.164
THF	388	463	4175	30730	0.029	0.59	6.95	37.4	0.210	0.210
Ethyl Acetate	386	470	4630	27280	0.047	0.56	6.75	38.1	0.199	0.230
Acetonitrile	388	477	4809	27950	0.090	0.58	6.93	45.6	0.304	0.472
Chloroform	388	464	4221	28770	0.050	0.73	7.77	39.1	0.148	0.259
DMF	395	484	4655	26980	0.102	0.53	6.65	43.8	0.274	0.404
Butanol	400	484	4339	26940	0.057	0.55	6.81	50.2	0.263	0.506
Propanol	400	485	4381	25780	0.060	0.55	6.83	49.2	0.274	0.570
Ethanol	402	486	4299	28420	0.062	0.57	7.00	51.9	0.288	0.654
Methanol	400	489	4550	30500	0.044	0.63	7.31	55.4	0.308	0.762

betain dye. In this method, change in dipole moment is calculated by correlating the Stokes shift of the fluorophore to E_T^N (Fig. 5) according to Eq. (8).

$$\Delta\bar{\nu} = 11307.6\left(\frac{\Delta\mu}{\Delta\mu_D}\right)^2\left(\frac{a_D}{a}\right)^3 E_T^N + Const. \quad (8)$$

$\Delta\mu$ is the difference between the excited and ground state dipole moments of the probe molecule and $\Delta\mu_D$ is the change in the dipole moment of the betaine dye; a (taken as 4.34 Å) and a_D are the Onsager cavity radiia of the probe molecule and betaine molecule respectively. Since the values of a_D and μ_D are known (6.2 Å and 9 Debye, respectively) the change in dipole moment is calculated using Eq. (9),

$$\Delta\mu = \left[\frac{81m}{(6.2/a)^3 \times 11307.6}\right]^{1/2} \quad (9)$$

where, m is the slope of linear plot of E_T^N *vs* Stokes shift (Fig. 5) and the value for $\Delta\mu$ is found to be 5.89 D. The higher value of $(\mu_e - \mu_g)$ suggest that the emissive state of MPNP is of strong ICT character. The value of $\Delta\mu$ obtained by Lippert-Mataga's equation is higher than that obtained by dimensionless microscopic solvent polarity parameters E_T^N, because in Lippert's plot only the dipole-dipole interactions are taken into

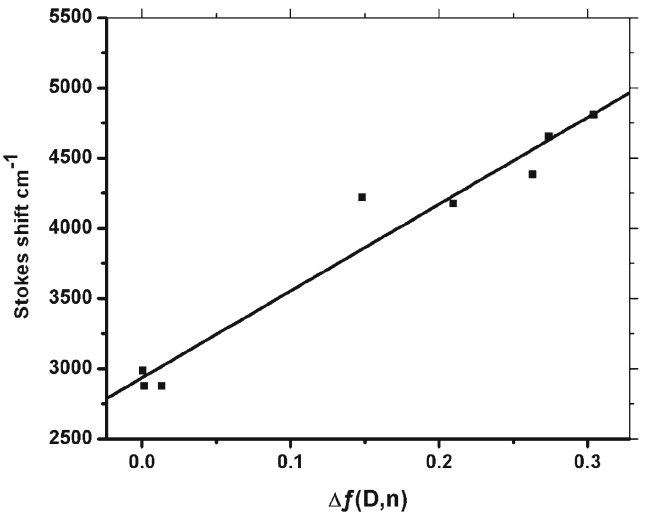

Fig. 4 Plot of Δf versus Stokes Shift (cm^{-1})

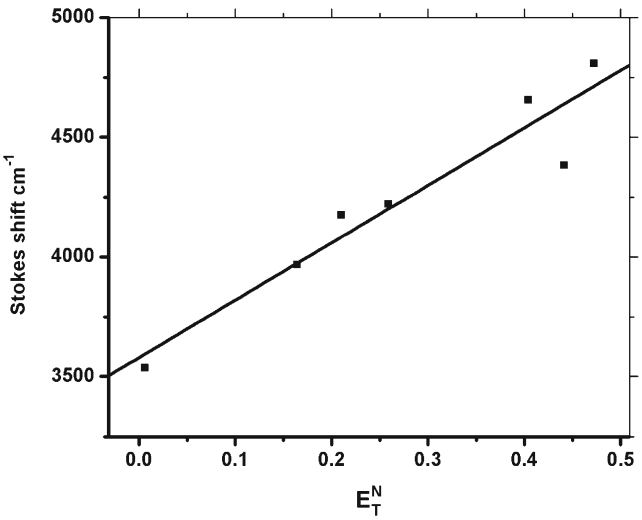

Fig. 5 Plot of E_T^N versus Stokes shift (cm^{-1})

account and does not consider the polarizability of solute molecules.

The ground to excited state transition dipole moment (μ_{12}) of MPNP in different solvents was calculated using Eq. (10) [33]:

$$\mu_{12}{}^{2} = \frac{f}{4.72 \times 10^{-7} E_{max}} \quad (10)$$

where, E_{max} is the energy maximum absorption in cm^{-1} and f is the oscillator strength which shows the effective number of electrons whose transition from ground to excited state gives the absorption area of the electronic spectrum. The experimental oscillator strength values were calculated using Eq. (11) [34],

$$f = 4.32 \times 10^{-9} \int \varepsilon(\bar{\nu})\, d\bar{\nu} \quad (11)$$

where, ε is the numerical value for molar decadic extinction coefficient measured in $dm^3\ mol^{-1}\ cm^{-1}$ and $\bar{\nu}$is the numerical value of the wave number measured in cm^{-1}. The values of f and μ_{12} are listed in Table 1 and indicate that the $S_o \rightarrow S_1$ transition is strongly allowed.

Fluorescence Quantum Yield of MPNP in Different Solvents

The fluorescence quantum yield can be correlated with $E_T(30)$ of the solvent, where $E_T(30)$ is the solvent polarity parameter introduced by Reichardt [31] that considers interactions such as solvent polarizability and hydrogen bonding besides those of a specific nature. The fluorescence quantum yield (ϕ_f) of MPNP is strongly influenced by the polarity and hydrogen bonding ability of the solvents as shown in Table 1. As depicted in Fig. 6, ϕ_f increases with increase in the polarity of the solvent (expressed as $E_T(30)$); reaching maximum in polar aprotic solvents like DMF and DMSO with a drop on further increase in the solvent polarity such as in alcoholic solvents. The increase in ϕ_f (negative solvatokinetic effect) with charge transfer character was explained by several mechanisms such as proximity effect and conformational changes [35]. Hydrogen bonding between solvent molecules and the carbonyl group of fluorophore is accounted for the reduction of ϕ_f in highly protic alcoholic solvents due to enhanced radiationless processes [26, 36].

Fluorescence Quenching Study of MPNP by Silver Nanoparticles

The nature of molecular interaction and microenvironment of fluorophores in solution can be studied by fluorescence quenching experiments. Interaction of silver nanoparticles with MPNP was investigated by fluorescence quenching measurements with variable concentrations of Ag NPs in ethanol and ethylene glycol. The emission spectra of 1×10^{-5} mol L^{-1} solution of MPNP in ethanol and ethylene glycol with different concentrations of Ag NPs are shown in Fig. 7a and b, respectively. On increasing the concentration of Ag NPs, the emission spectrum of MPNP remains unaltered in wavelength but a substantial decrease in fluorescence intensity was observed; which rules out the possibility of ground state complex formation between MPNP and Ag NPs.

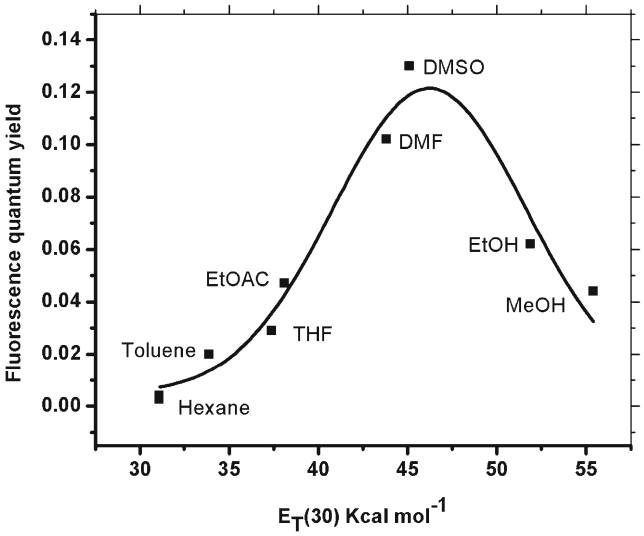

Fig. 6 Plot of $E_T(30)$ versus fluorescence quantum yield

The Stern-Volmer quenching constant (K_{sv}) for MPNP using Ag NPs as quencher were obtained from the Stern-Volmer Eq. (12) [25]:

$$\frac{I_o}{I} = 1 + K_{sv}[Ag^o] \quad (12)$$

where I_o and I are the fluorescence intensities in the absence and presence of the quencher concentration [Ag^o] The Stern-Volmer plot for MPNP (Fig. 8) was found to be linear with correlation coefficient (R^2) equal to 0.97 and 0.99 in ethanol and ethylene glycol, respectively. From the slopes of the linear plots, K_{gv} values were calculated as $1.51 \times 10^9\ M^{-1}$ and $3.48 \times 10^9\ M^{-1}$ in ethanol and ethylene glycol, respectively. The higher value for K_{sv} in ethylene glycol implies that quenching efficiency increases as the medium viscosity increases and quenching process is not completely diffusion controlled. The significant overlap between the emission spectrum of MPNP with the absorption of spectrum of Ag NPs (Fig. 9) reveal the possibility of non-radiative energy transfer from MPNP to Ag NPs according to Förster's theory [37]. Thus, the Stern-Volmer plot and the spectral overlap between the MPNP and Ag NPs indicate the dynamic nature of the quenching process.

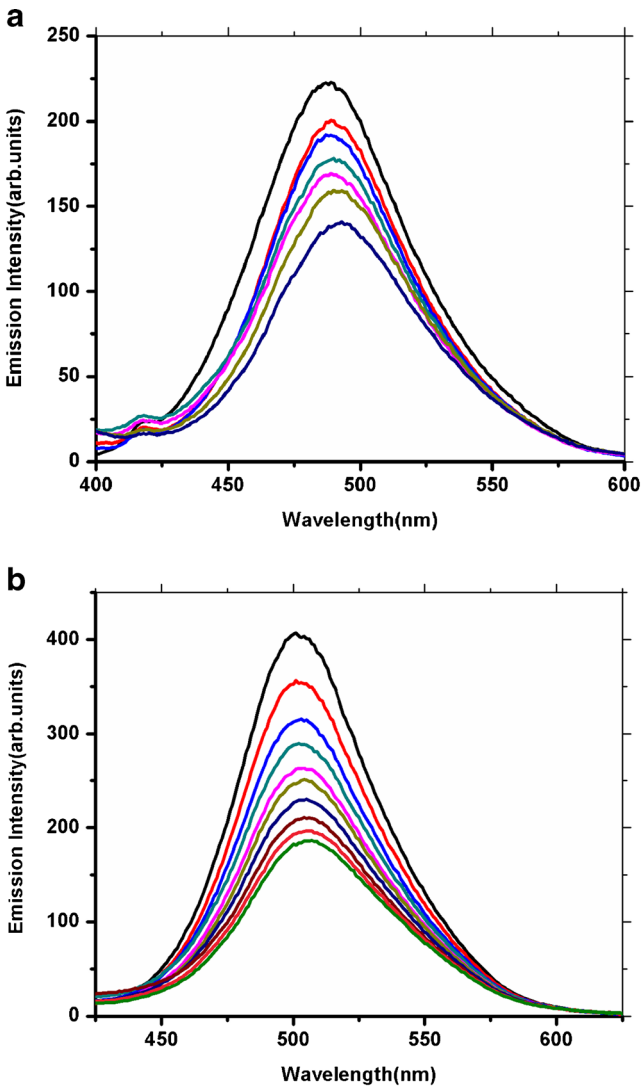

Fig. 7 (**a**) Emission spectra of 1×10^{-5} mol L^{-1} of MPNP in EtOH in presence of different concentrations of Ag NPs . The concentrations of Ag NPs at decreasing emission intensity are 0.0, 39, 78, 156, 195, 273, and 351 pM (λ_{ex}=380 nm). (**b**) Emission spectra of 1×10^{-5} mol L^{-1} of MPNP in ehtylene glycol in presence of different concentrations of Ag NPs . The concentrations of Ag NPs at decreasing emission intensity are 0.0, 39, 78, 117, 156, 195, 234, 273, 312 and 351 pM (λ_{ex}=380 nm)

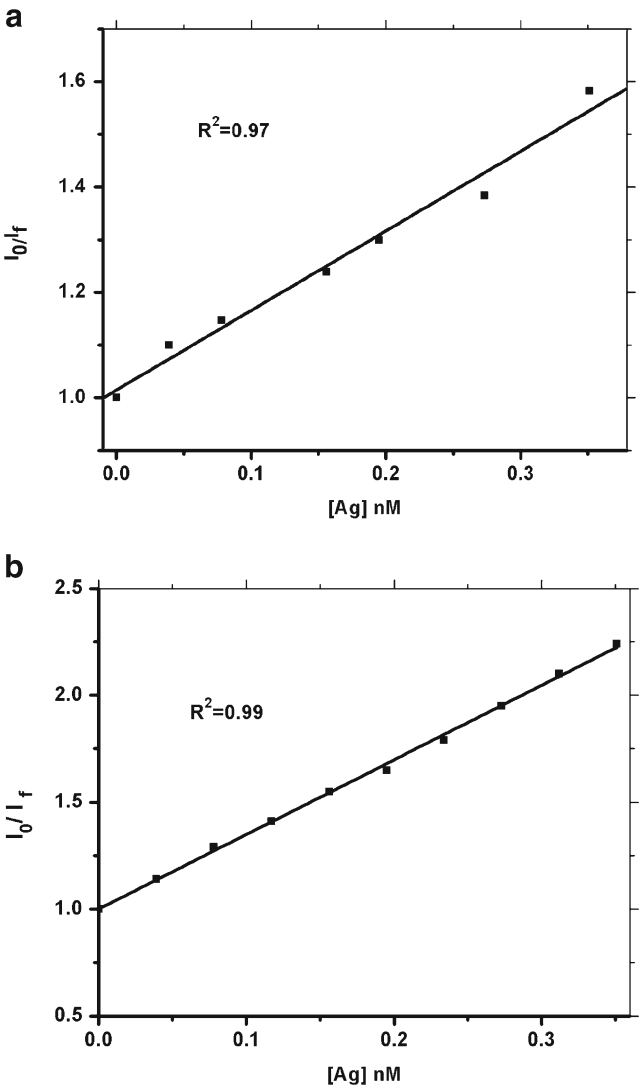

Fig. 8 (**a**) Stern – Volmer plot for fluorescence quenching of MPNP by Ag NPs in ethanol. (**b**) Stern – Volmer plot for fluorescence quenching of MPNP by Ag NPs in ethylene glycol

The interaction between adsorbed and unadsorbed MPNP molecules was further investigated by determining the apparent association constant (K_{app}) using Benesi–Hildebrand method [38], Eqs. (13–15).

$$\mathrm{MPNP} + \mathrm{Ag} \rightarrow [\mathrm{MPNP} \cdots\cdots \mathrm{Ag}] \tag{13}$$

$$\mathrm{Kapp} = [\mathrm{MPNP} \cdots \mathrm{Ag}]/[\mathrm{MPNP}][\mathrm{Ag}] \tag{14}$$

$$\frac{1}{F^{o}-F} = \frac{1}{(F^{o}-F')} + \frac{1}{k_{app}} \times \frac{1}{(F^{o}-F')[Ag]} \tag{15}$$

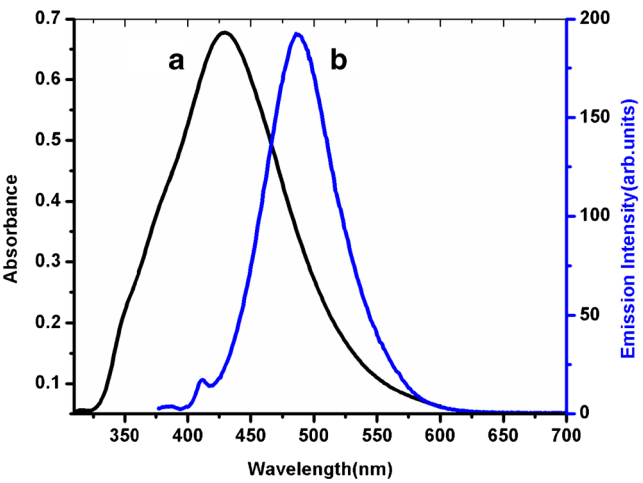

Fig. 9 Spectral overlap of (**a**) absorption spectrum of silver nanoparticles with (**b**) emission spectrum of MPNP

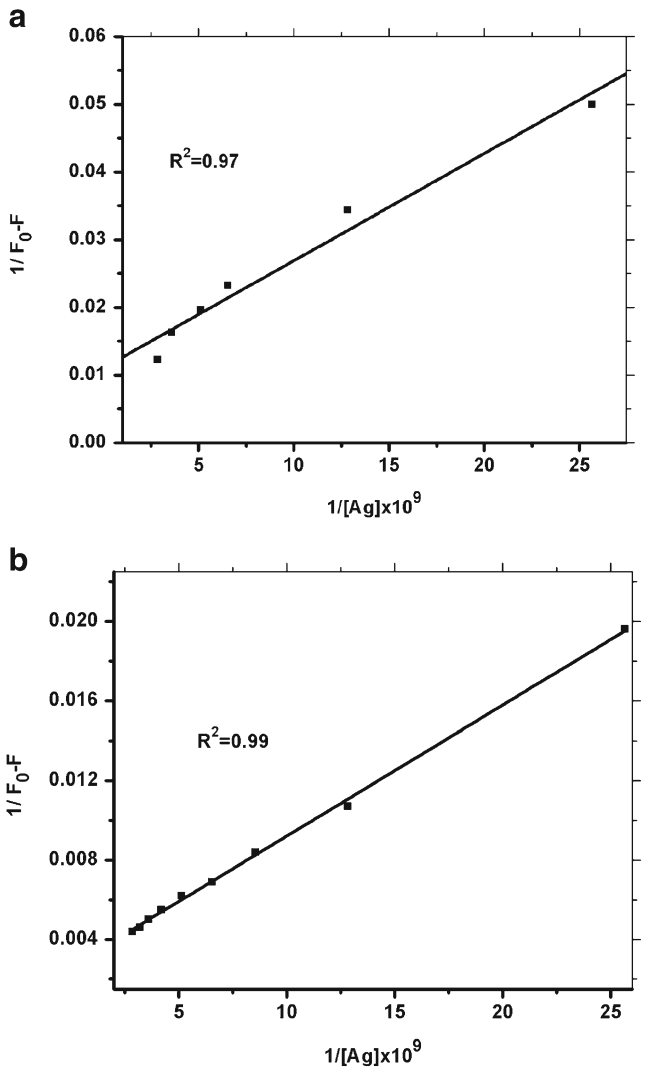

Fig. 10 Benesi – Hildebrand plot for the adsorption of MPNP on Ag NPs: (**a**) in ethanol and (**b**) in ethylene glycol

where, K_{app} is the apparent association constant, F^0 is the initial fluorescence intensity of dye molecules, F' is the fluorescence intensity of Ag adsorbed dye and F is the observed fluorescence intensity at its maximum. The calculated values of K_{app} obtained from the plot of $1/F^0$-F vs. 1/ [Ag] (Fig. 10) are found to be 6.98×10^9 and 3.97×10^9 M^{-1} for ethanol and ethylene glycol, respectively. The higher value of K_{app} indicates the strong association between the MPNP and Ag NPs.

Crystal Structure Studies

MPNP molecule was crystallized in chloroform with the space group $P2_1/a$ (No. 14) and contains naphthalene and a pyrrole ring in its skeleton. This structural study along with the other physical studies was carried out, with the aim, to know the three dimensional behavior and Vander Walls interactions of molecules in a unit cell. The crystallographic data and refinement parameters are summarized in Table S1 (supporting information) with bond lengths and bond angles are provided in Tables S2 and S3 (supporting information). The naphthalene and pyrrole moieties are twisted at dihedral angle of 8.29 (1)°. The molecules are further connected by weak C-H…O interactions to form inversion dimers via the formation of 16 membered ring motif R^1_1 (16) [39] as shown in Fig. 11. The oxygen atom O1 is situated at (1-x, 2-y, −z) with respect to the donor carbon atoms (C18) at (x, y, z) via H18B.

Conclusion

In summary, we have synthesized a new pi-conjugated electron donor-acceptor type chalcone derivative MPNP having

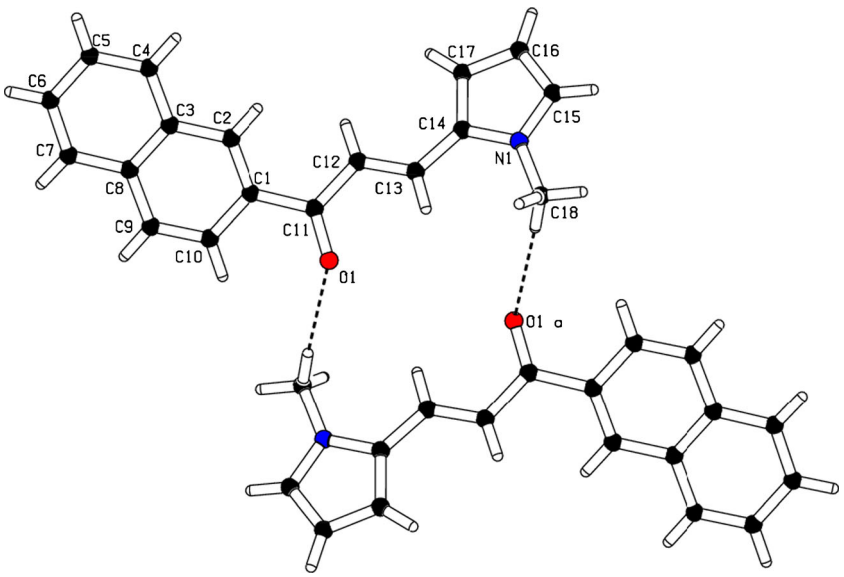

Fig. 11 Labelled diagram of MPNP showing inter molecular hydrogen bonding using dashed lines

intramolecular charge transfer (ICT) characteristics. The structure of this compound was identified by spectroscopy and single crystal X-ray crystallography. A red shift in the emission spectrum of MPNP was observed upon increasing the solvent polarity, due to intramolecular charge transfer and inter-molecular hydrogen bonding between solute and solvent. Dipole moment calculation results suggest that the excited state of MPNP is more polar than the ground state. Physicochemical parameters such as molar absorptivity, oscillator strength, transition dipole moment and fluorescence quantum yield of MPNP have been calculated. The fluorescence quenching of MPNP by colloidal silver nanoparticles in ethanol and ethylene glycol have also been studied. From the fluorescence quenching data, dynamic quenching and energy transfer from excited MPNP to Ag NPs play a major role in the fluorescence quenching of MPNP by Ag NPs.

Acknowledgments The authors thank the Center of Excellence for Advanced Materials Research and Department of Chemistry at King AbdulAziz University for providing the research facilities. One of the authors, Mehboobali Pannipara is grateful to Deanship of Graduate Studies, King Abdulaziz University for providing PhD Fellowship.

References

1. El-Daly SA, Asiri AM, Alamry KA, Khan SA (2013) Spectroscopic studies and laser activity of 3-(4-dimethylamino-phenyl)-1-(2,5-dimethyl-furan-3-yl)-propenone (DDFP): A new green laser dye. J Lumin 137:6–14
2. Singh H, Sindhu J, Khurana JM (2014) Determination of dipole moment, solvatochromic studies andapplication as turn off fluorescence chemosensor of new3-(4-(dimethylamino) phenyl)-1-(5-methyl-1-(naphthalen-1-yl)-1H-1,2,3-triazol-4-yl) prop-2-en-1-one. Sensors Actuators B 192:536–542
3. Rahulan KM, Balamurugan S, Meena KS, Yeap GY, Kanakam CC (2014) Synthesis and nonlinear optical absorption of novel chalcone derivative compounds. Opt Laser Technol 56:142–145
4. Nagarajan N, Prakash A, Velmurugan G, Shakti N, Katiyar M, Venuvanalingam P, Renganathan R (2014) Synthesis, characterisation and electroluminescence behaviour of π-conjugated imidazole–isoquinoline derivatives. Dyes Pigments 102:180–188
5. Işık D, Santato C, Barik S, Skene WG (2012) Charge-carrier transport in thin films of π-conjugated thiopheno-azomethines. Org Electron 13(12):3022–3031
6. Mishra A, Bäuerle P (2012) Small molecule organic semiconductors on the move: promises for future solar energy technology. Angew Chem Int Ed 51(9):2020–2067
7. SunY CH, Cao D, Liu Z, Chen H, Deng Y, Fang Q (2012) Chalcone derivatives as fluorescence turn-on chemosensors for cyanide anions. J Photochem Photobiol A Chem 244:65–70
8. Poornesh P, Shettigar S, Umesh G, Manjunatha KB, Prakash Kamath K, Sarojini BK, Narayana B (2009) Nonlinear optical studies on 1, 3-disubstituent chalcones doped polymer films. Opt Mater 31(6):854–859
9. Rajashekara B, Sowmendranb P, Siva Sankara Sai S, Nageswara Rao G (2012) Synthesis, characterization and two-photon absorption based broadband optical limiting in diarylideneacetone derivative. J Photochem Photobiol A Chem 238:20–23
10. Chhabra R, Sharma J, Wang H, Zou S, Lin S, Yan H, Liu Y (2009) Distance-dependent interactions between gold nanoparticles and fluorescent molecules with DNA as tunable spacers. Nanotechnology 20(48):485201
11. Daniel MC, Astruc D (2004) Gold nanoparticles: assembly, supramolecular chemistry, quantum-size-related properties, and applications toward biology, catalysis, and nanotechnology. Chem Rev 104(1):293–346
12. Deng W, Goldys EM (2012) Plasmonic approach to enhanced fluorescence for applications in biotechnology and the life sciences. Langmuir 28(27):10152–10163
13. Hong B, Kang KA (2006) Biocompatible, nanogold-particle fluorescence enhancer for fluorophore mediated, optical immunosensor. Biosens Bioelectron 21(7):1333–1338
14. Ng MY, Liu WC (2009) Fluorescence enhancements of fiber-optic biosensor with metallic nanoparticles. Opt Express 17(7):5867–5878
15. Fu Y, Zhang J, Lakowicz JR (2007) Plasmonic enhancement of single-molecule fluorescence near a silver nanoparticle. J Fluoresc 17(6):811–816
16. Kalele S, Deshpande AC, Singh SB, Kulkarni SK (2008) Tuning luminescence intensity of RHO6G dye using silver nanoparticles. Bull Mater Sci 31(3):541–544
17. Rainò G, Stöferle T, Park C, Kim HC, Topuria T, Rice PM, Mahrt RF (2011) Plasmonic nanohybrid with ultrasmall Ag nanoparticles and fluorescent dyes. ACS Nano 5(5):3536–3541
18. Swierczewska M, Lee S, Chen X (2011) The design and application of fluorophore–gold nanoparticle activatable probes. Phys Chem Chem Phys 13(21):9929–9941
19. Maxwell DJ, Taylor JR, Nie S (2002) Self-assembled nanoparticle probes for recognition and detection of biomolecules. J Am Chem Soc 124(32):9606–9612
20. Chung HY, Leung PT, Tsai DP (2013) Molecular fluorescence in the vicinity of a charged metallic nanoparticle. Opt Express 21(22): 26483–26492
21. El-Daly SA, Asiri AM, Obeid AY, Khan SA, Alamry KA, Hussien MA, Al-Sehemi AG (2013) Photophysical parameters and laser activity of 3 (4-dimethylamino-phenyl)-1-(2, 5-dimethyl-thiophen-3-yl)-propenone (DDTP): A new potential laser dye. Opt Laser Technol 45:605–612
22. Sheldrick GM (2007) A short history of SHELX. Acta Crystallogr A: Found Crystallogr 64(1):112–122
23. Barbour LJ (2001) X-seed— a software tool for supramolecular crystallography. J Supramol Chem 1(4):189–191
24. Lee PC, Meisel D (1982) Adsorption and surface-enhanced Raman of dyes on silver and gold sols. J Phys Chem 86(17):3391–3395
25. Lakowicz JR (2006) Principles of fluorescence spectroscopy, 3 rd ed. Springer, New York
26. Jana S, Dalapati S, Ghosh S, Guchhait N (2013) Excited state intramolecular charge transfer process in 5-(4-dimethylamino-phenyl)-penta-2,4-dienoic acid ethyl ester and effect of acceptor functional groups. J Photochem Photobiol A Chem 261:31–40
27. Shaikh M, Pal H (2014) Photophysics of donor–acceptor kind of styryl dyes: Involvement of twisted intramolecular charge transfer (TICT) state and the effect of solvent polarity. J Spectrosc Dyn 4:1–12
28. Lippert E (1957) Spectroscopic determination of the dipole moment of aromatic compounds in the first excited singlet state. Z Elektrochem 61:962–975
29. Mataga N, Kubota T (1970) Molecular interactions and electronic spectra. Marcel Dekker, New York, pp 371–410
30. Suppan P (1983) Excited-state dipole moments from absorption/fluorescence solvatochromic ratios. Chem Phys Let 94:272–275
31. Reichardt C (1994) Solvatochromic dyes as solvent polarity indicators. Chem Rev 94(8):2319–2358
32. Ravi M, Soujanya T, Samanta A, Radhakrishnan TP (1995) Excited-state dipole moments of some Coumarin dyes from a solvatochromic method using the solvent polarity parameter, ENT. J Chem Soc Faraday Trans 91(17):2739–2742

33. Coe BJ, Harris JA, Asselberghs I, Clays K, Olbrechts G, Persoons A, Hupp JT, Johnson RC, Coles SJ, Hursthouse MB, Nakatani K (2002) Quadratic nonlinear optical properties of *N*-Aryl stilbazolium dyes. Adv Funct Mater 12:110–116
34. Gordon P, Gregory P (1987) Organic chemistry in colour. Chimia, Moskva
35. Rurack K, Dekhtyar MI, Bricks JL, Resch-Genger U, Retting W (1999) Quantum yield switching of fluorescence by selectively bridging single and double bonds in chalcones: involvement of two different types of conical intersections. J Phys Chem A 103:9626–1935
36. Birks JB (1970) Photophysics of aromatic molecules. Wiley Interscience, London, p 88
37. Förster T (1996). in: O. Sinanoglu (Ed.), Modern Quantum Chemistry, Academic Press, New York.
38. Benesi HA, Hildebrand JH (1949) A spectrophotometric investigation of the interaction of iodine with aromatic hydrocarbons. J Am Chem Soc 71:2703–2707
39. Bernstein J, Davis RE, Shimoni L, Chang NL (1995) Patterns in hydrogen bonding: functionality and graph Set analysis in crystals. Angew Chem Int Ed Engl 34:1555–1573